Inertial particle impaction on a cylinder in turbulent cross-flow at modest Reynolds numbers

Jørgen R. Aarnes [a,*], Nils E.L. Haugen [a,b], Helge I. Andersson [a]

[a] *Department of Energy and Process Engineering, Norwegian University of Science and Technology, Trondheim, Norway*
[b] *SINTEF Energy Research, Trondheim Norway*

ABSTRACT

Particle impaction on a cylinder in a cross-flow is investigated with the use of Direct Numerical Simulations, with focus on the effect of free-stream turbulence on the front-side impaction efficiency. The turbulence considered is high-intensity homogeneous isotropic turbulence, introduced upstream of the cylinder in moderate Reynolds number flows. It is found that the free-stream turbulence leads to a significant increase in the number of particles that impact the cylinder for certain Stokes numbers (St). The peak amplification of impaction is observed at $St = 0.3$, for different integral scales and Reynolds numbers. This peak is related to a change in impaction mechanism, from boundary stopping to boundary interception, and it will therefore depend on the size of the particles as well as on the Stokes number. Using statistical analysis, an expectation value of predicted effects of free-stream turbulence on particle impaction is derived. This expression predicts the observed impaction amplification to a good degree, particularly in terms of which Stokes numbers that are affected by the turbulence.

© 2018 Elsevier Ltd. All rights reserved.

1. Introduction

Particle laden fluid flows are common both in nature and in a large number of industrial applications. In many applications the impaction between particles and solid objects entrained in the fluid flow is central. Such impactions may lead to the buildup of a deposition layer on the solid-fluid interface or to erosion of the solid object. In industry, these mechanisms are typically found in filters, furnaces, industrial boilers and ventilation systems.

A simple cylindrical geometry may well approximate the solid objects in several of the applications mentioned above, and a cylinder in a cross-flow has become a benchmark case for particle impaction. Inertial particle impaction on a cylinder in a cross-flow can be split into three different impaction modes, based on what drives the trajectories of the convected particles during impact. The modes are classical impaction (particle inertia driven trajectory), boundary stopping (boundary layer driven trajectory) and boundary interception (mass center of particles do not come in contact with the cylinder) (cf. Haugen and Kragset, 2010; Weber et al., 2013b). The dominant mode is determined by both the particle's size and its Stokes number (with some dependence on Reynolds number). Here we define the Stokes number as the ratio of the particle Stokes time to the timescale of the fluid flow around the solid object ($St = \tau_p/\tau_f$). The Reynolds number is $Re = U_0 D/\nu$, where U_0 is the free-stream velocity, D is the cylinder diameter and ν is the kinematic viscosity. Generally, classical impaction occurs for Stokes numbers $St \gtrsim 0.9$, boundary stopping for $0.2 \lesssim St \lesssim 0.9$ and boundary interception for $St \lesssim 0.2$. Note that the boundary stopping mode is partly overtaken by the classical impaction mode for high Reynolds numbers (see Haugen and Kragset, 2010).

Potential flow theory can be used to calculate the particle impaction efficiencies as a function of particle size (see Israel and Rosner, 1982). The method is well accepted for Stokes numbers larger than unity. Rotational and viscous flow effects are not resolved with a potential flow approximation. These are particularly important for transport of particles with small Stokes numbers, as these follow the flow to a large extent. Further, the approximation assumes infinitesimal particles sizes, and will therefore not account for boundary interception. Consequently, no impaction occurs for particles with $St < St_{\text{crit}} = 1/8$ (Ingham et al., 1990) (note that viscous effects will increase the value of St_{crit}, hence St_{crit} is larger for smaller Reynolds numbers (see Phillips and Kaye, 1999).

Other approaches to finding the impaction efficiencies, using experimental (Schweers et al., 1994; Kasper et al., 2009), numerical (Yilmaz et al., 2000; Li et al., 2008; Haugen and Kragset, 2010; Haugen et al., 2013) and phenomenological modeling (Huang et al., 1996) are found in literature. With few exceptions, these studies regard smooth laminar flow past one or more cylinders. It is,

however, reasonable to expect that the influence of any turbulence in the flow is highly relevant for the rate of particle impaction in the mentioned applications. The turbulence in said applications can be due to, e.g., transitional eddies in the free shear layers of the cylinder at high Reynolds numbers, combustion upstream of the cylinder, wall turbulence for a cylinder in a confined space, or similar sources. Either way, one would expect the velocity fluctuations to affect the inertial particle impactions on the cylinder surface.

An exception to the experimental studies on particles in smooth laminar flow, is the measurements by Douglas and Ilias (1988) on the effect of turbulence on particle impaction. In that study the cylinder was situated within a channel such that the turbulence was generated by the channel walls. The results showed increased impaction efficiencies when turbulence was present in the flow, and eddy diffusion was considered as a prime mechanism leading to this. The scatter in the data was, however, quite large for small Stokes numbers.

Numerical studies on particle impaction in turbulent flows are often limited by the fact that they use Reynolds-Averaged Navier–Stokes modeling of the turbulence (see review by Weber et al., 2013a). One such study was performed by Weber et al. (2013b), in which it was found that the turbulence played a minor role for particles with Stokes number larger than St_{crit} and had the effect of increasing the particle impactions below this critical point. However, as pointed out by the authors of said study, the predictable power of these CFD-simulations is limited by the lack of rigorous testing of the particle tracking procedure in use. Further limitations are introduced from the modeling and time-averaging of the flow, as seen by the factor two difference in impaction efficiency for small particles when switching between turbulence modeled by the $k - \epsilon$ model and Reynolds Stress Models.

In the current study, we consider the effect of turbulence in the flow on the particle impaction efficiencies on a circular cylinder by using Direct Numerical Simulations (DNS), i.e., three-dimensional simulations where all scales of the turbulence (spatial and temporal) are resolved. The turbulence is not generated in the flow past the cylinder, as the Reynolds numbers in our study are too low for this. Rather, free-stream turbulence is inserted upstream of the cylinder and decays as it is convected by the mean flow. This typically emulates the flow regime above a thermal incinerator or boiler for solid fuels. As particles impact they deposit on the cylinder surface. The aim of this study is to understand the way the turbulence affects the inertial impaction mechanism of the particles.

The structure of the paper is the following: In Section 2 the governing flow equation and particle equations are given, and the simulation set-up is described. Following this, different ways to predict the effects of turbulence on the particle impaction is described in Section 3. Results from simulations with and without free-stream turbulence are presented in Section 4, and compared to predicted amplification of particle impaction, before conclusions are drawn in Section 5.

2. Methodology

2.1. Governing equations

The equations describing the flow are the equation for continuity,

$$\frac{D\rho}{Dt} = -\rho \nabla \cdot \boldsymbol{u}, \tag{1}$$

and momentum,

$$\rho \frac{D\boldsymbol{u}}{Dt} = -\nabla p + \nabla \cdot (2\mu \boldsymbol{S}), \tag{2}$$

where ρ, t, $\boldsymbol{u}$ and p are the density, time, velocity vector and pressure, respectively, $\mu = \rho \nu$ is the dynamic viscosity and

$$\frac{D}{Dt} = \frac{\partial}{\partial t} + \boldsymbol{u} \cdot \nabla \tag{3}$$

is the substantial derivative operator. The rate of strain tensor is given by:

$$\boldsymbol{S} = \frac{1}{2}\left(\nabla \boldsymbol{u} + \left(\nabla \boldsymbol{u}\right)^T\right) - \boldsymbol{I}\left(\frac{1}{3}\nabla \cdot \boldsymbol{u}\right), \tag{4}$$

where $\boldsymbol{I}$ is the identity matrix. The pressure is computed by the isothermal ideal gas law, $p = c_s^2 \rho$, where c_s is the speed of sound. The flow is isothermal and weakly compressible.

Particles in the flow are point particles. A Lagrangian formalism is used to track the particles. A particle's velocity and position is described by:

$$\frac{d\boldsymbol{v}_p}{dt} = \frac{\boldsymbol{F}_{D,p}}{m_p}, \tag{5}$$

$$\frac{d\boldsymbol{x}_p}{dt} = \boldsymbol{v}_p, \tag{6}$$

where $\boldsymbol{v}_p$, $\boldsymbol{x}_p$ and m_p are the velocity, center of mass position and mass of the particle, respectively. The drag force acting upon a particle is given by:

$$\boldsymbol{F}_{D,p} = \frac{1}{2C_c}\rho C_{D,p}A_p|\boldsymbol{u} - \boldsymbol{v}_p|(\boldsymbol{u} - \boldsymbol{v}_p), \tag{7}$$

where $A_p = \pi d_p^2/4$ is the cross sectional area of the particle and

$$C_c = 1 + \frac{2\lambda}{d_p}\left(1.257 + 0.4e^{(-1.1d_p/2\lambda)}\right), \tag{8}$$

is the Stokes–Cunningham factor with parameters set for air for a particle with diameter d_p (Cunningham, 1910; Davies, 1945). The mean free path λ accounts for the fact that for very small particles, the surrounding medium can no longer be regarded as a continuum but, rather, distinct particles. The particle drag coefficient is given by:

$$C_{D,p} = \frac{24}{Re_p}\left(1 + 0.15Re_p^{0.687}\right). \tag{9}$$

The expression is valid for particles with particle Reynolds number $Re_p = d_p|\boldsymbol{v}_p - \boldsymbol{u}|/\nu \lesssim 1000$, which is the case for all particles in the present study. Thus, the particle drag force can be written as:

$$\boldsymbol{F}_{D,p} = \frac{m_p}{\tau_p}(\boldsymbol{u} - \boldsymbol{v}_p), \tag{10}$$

where

$$\tau_p = \frac{Sd_p^2 C_c}{18\nu(1 + f_c)} \tag{11}$$

is the particle response time, $f_c = 0.15Re_p^{0.687}$ and $S = \rho_p/\rho$. Note that Eq. (11) equals the Stokes time in the limit $C_c = 1$ and $Re_p \ll 1$. The Stokes number ($St = \tau_p/\tau_f$) is defined with a fluid time scale

$$\tau_f = \frac{D}{2U_0}. \tag{12}$$

An alternative convention is to define the Stokes number without a factor two in the denominator of the fluid time scale.

2.2. Simulations

The simulations were performed with the high-order finite-difference code for compressible hydrodynamic flows known as The Pencil Code (see Brandenburg and Dobler, 2002; The Pencil Code, 2018). The equations describing the flow are discretized with
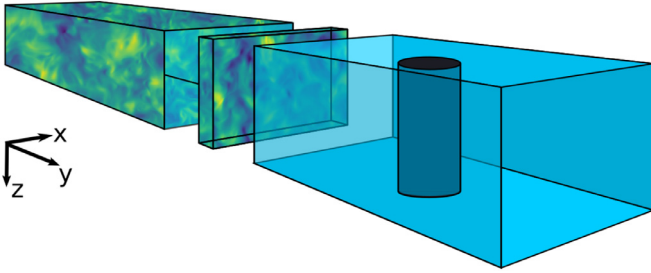
Fig. 1. Computational domain, split into two rectangular boxes. Left box for turbulence generation and right box for flow domain. Thin slices of velocity data are taken from the turbulence domain and added to the inlet of the flow domain, illustrated here by a thin rectangular box between the two domains. The slice thickness and the cylinder in the flow domain are not to scale.

Table 1
Turbulence intensity T_i at different positions along the streamwise direction in a 12D long domain, with no cylinder present in the flow.

Position	$Re = 100$		$Re = 400$	
(downstream)	$\Lambda = 2.7D$	$\Lambda = 0.8D$	$\Lambda = 2.7D$	$\Lambda = 0.8D$
0	0.230	0.222	0.232	0.225
3D	0.172	0.090	0.203	0.143
6D	0.152	0.061	0.183	0.106
9D	0.139	0.048	0.169	0.086

a memory efficient third-order Runge–Kutta method in time (developed by Williamson, 1980) and sixth-order central differencing in space. A three-point deep ghost-zone immersed boundary method was used to resolve the cylinder surface, with ghost-points set by no-slip and impermeability boundary conditions along grid lines (with quadratic interpolation) and zero gradient of the density along the surface normal (with linear interpolation). For details on the numerical method, and grid and time independence tests, see Aarnes et al. (2018).

The fluid velocities used to update the particle trajectories were interpolated from surrounding grid points by tri-linear Lagrangian interpolation. In the immediate vicinity of the cylinder surface, quadratic interpolation was used to compute the velocity component normal to the surface.

2.2.1. Fluid flow and turbulence generation

The computational domain consists of two rectangular boxes: a turbulence production domain and a flow domain (see Fig. 1). The production domain is a periodic box in which homogeneous isotropic turbulence was generated by external forcing in random directions over a selected range of wave numbers. The strength of the forcing and the wavenumber range are free parameters which determine the turbulence intensity and length scale, respectively. For details, see Brandenburg (2001); Haugen and Brandenburg (2006) and Aarnes et al. (2018). The flow domain is a rectangular box with periodicity in two direction (x- and z-direction), and a mean flow in the third direction (y-direction). Navier–Stokes characteristic boundary conditions (NSCBC) were used both at the inlet and at the outlet of the flow domain. This boundary formulation is a formulation that makes use of one-dimensional characteristic wave relations to allow acoustic waves to pass through the boundaries (Poinsot and Lele, 1992). The NSCBC implementation in the Pencil Code uses modifications suggested by Yoo et al. (2005) and Lodato et al. (2008) to account for transversal flow effects, e.g. for turbulent flow at the inlet. A circular cylinder is placed in the center of the flow domain, with axis along the z-direction. Simulations were performed for flow in the unsteady vortex-shedding regime, with Reynolds numbers $Re = 100$ and $Re = 400$.

The size of both the turbulence production domain and the flow domain is $(L_x, L_y, L_z) = (6D, 12D, 4D)$, where D is the cylinder diameter. The domain size was set sufficiently large to resolve the three-dimensional phenomena in the flow (the wavelength of instabilities in the cylinder wake is approximately 1D in the z-direction at $Re = 400$ Williamson, 1996). Validation runs have been performed, and a uniform grid spacing of $D/\Delta x = 40$ and $D/\Delta x = 64$ for flow with $Re = 100$ and $Re = 400$, respectively, was deemed sufficiently accurate to fully resolve all scales of the free-stream turbulence and the boundary layer around the cylin-

der. The grid spacing did, however, limit the particle Stokes numbers which could be used to $St \geq 0.2$. Smaller particles require a finer resolution in order to be represented accurately in the vicinity of the cylinder, as the interpolation of fluid velocities for use in Eq. (10) is sensitive to the grid spacing. Very small, tracer-like particles are particularly sensitive to incorrect estimation of forces from the fluid on the particle, as being brought marginally closer to the surface may result in interception rather than no interception. Note that grid spacings $\Delta x = \Delta y = \Delta z$ were used, to ensure that the spatial Kolmogorov microscale (η_{Kol}) was resolved in all directions ($\Delta x / \eta_{\text{Kol}} = 3.48, 1.92$ for $Re = 100, 400$). The strict advective time step restriction ($\Delta t \leq C_u \Delta x / (|\boldsymbol{u}|_{max} + c_s)$, where C_u is the advective Courant number) due to the low Mach number ($Ma = 0.1$), ensured several hundred time steps per (temporal) Kolmogorov microscale. Sufficiently small time steps is crucial to accurately compute the particle trajectories. The strict time step restriction mentioned above ensured that $\Delta t \ll \tau_p$ for all particles in the simulations.

Once the forced turbulence was statistically stationary, slices of flow quantities from the turbulence domain were added to the inlet of the flow domain. The inlet velocity in the flow domain $\boldsymbol{U} = \langle \boldsymbol{U_0} \rangle + \boldsymbol{u}'$, with mean flow $\boldsymbol{U_0} = (0, U_0, 0)$ and the velocity fluctuations $\boldsymbol{u}'$. The velocity fluctuations at the inlet were updated at every time step using data from the turbulence domain. All input slices for a flow simulation came from the same time-snapshot of the turbulence domain. Based on Taylor's hypothesis, at time t the plane of the turbulence domain with a y-position of $y = (y_0 - U_0 t)$ was used as turbulent inlet condition. The mean velocity was not affected by the insertion of turbulence at the inlet.

In the flow domain, the turbulence decayed when convected downstream towards and past the circular cylinder. The decay rate of the turbulence depends on its intensity ($T_i = u_{\text{rms}} / \langle \boldsymbol{U} \rangle$ where u_{rms} is the root-mean-square value of the three-dimensional velocity fluctuations) and integral scale (Λ), and the Reynolds number of the flow. Turbulence with integral scale $\Lambda = 2.7D$ and $\Lambda = 0.8D$ was used, with intensity 0.22–0.23% at the inlet. For details on the turbulence decay, see Table 1, where T_i at selected points along the streamwise direction in a cylinder-free flow domain is listed, for the different Reynolds numbers and integral scales. Instantaneous velocity contours of the decaying turbulence at $Re = 400$ can be seen in Fig. 2.

2.2.2. Particles

Particles with Stokes numbers ranging from 0.2 to 10 were inserted at random positions within a thin box covering the inlet of the flow domain. The velocity of an inserted particle was initialized to the mean inlet velocity. Particles were removed from the simulations either when hitting the cylinder or when reaching the outlet boundary.

In each simulation, a large number of particles (1.0×10^7) over a selection of Stokes numbers were inserted at a constant rate of approximately $(1.25 \times 10^6)/\tau_K$, where τ_K is the shedding period of the von Kármán eddy street. This ensured that the particles interacted with the flow past the cylinder over several shedding cycles. The variation in Stokes number was achieved by varying the par-
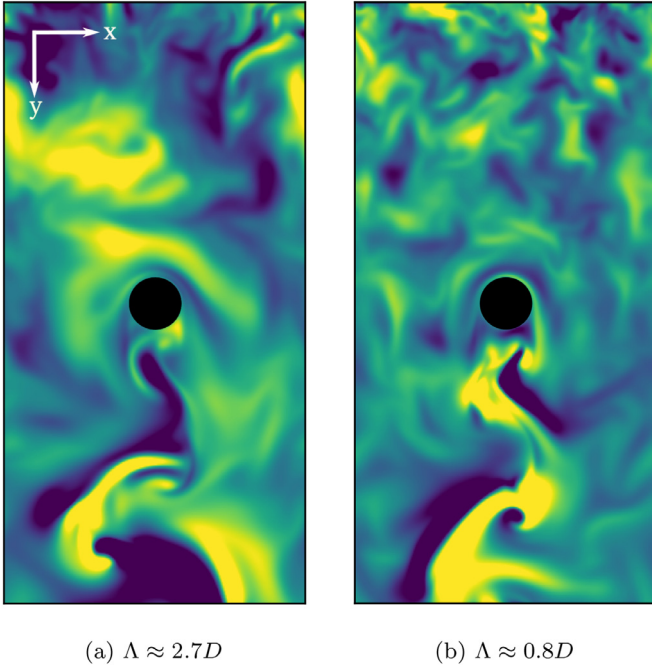
(a) $\Lambda \approx 2.7D$ (b) $\Lambda \approx 0.8D$

Fig. 2. Contours of velocity component normal to the plane of view, in a plane along the streamwise direction, perpendicular to the cylinder axis, with flow from top to bottom. High intensity free-stream turbulence with integrals scale Λ inserted at the top and convected downstream. Flow Reynolds number is 400. Dark blue (light yellow) corresponds to negative (positive) values. (For interpretation of the references to color in this figure legend, the reader is referred to the web version of this article.)

Table 2

Typical distribution of particles in a simulation. Stokes number greater or equal 2.0 include $St = 2.0, 3.0, 5.0$ and 10, each containing approximately 2.3% of the particles in the simulation.

St	0.2	0.3	0.4	0.5	0.6	0.7	0.8	0.9	1.0	≥ 2.0
N_{St}/N_{tot} (%)	14	13	12	12	9	9	9	6	6	9

ticle radii. For a given Stokes and Reynolds number, the particle diameter can be determined by:

$$\frac{d_p}{D} = 3\sqrt{\frac{St}{SRe}}. \tag{13}$$

In all simulations the ratio of particle to fluid density $S = \rho_p/\rho = 1000$.

The distribution of particles with respect to Stokes numbers was non-uniform. Since the impaction probability is a lot lower for particles with small St than high St, more particles were needed in the low than in the high St range in order to obtain good statistics of the impaction rate. To illustrate this, consider that even with 14% of the inserted particles having $St = 0.2$ and only 2.3% having $St = 10$, approximately 250 times more particles with $St = 10$ impact the cylinder than with $St = 0.2$. The particle distribution for a typical simulations is given in Table 2.

3. Estimated effects of turbulence on particle impaction

When turbulence is introduced at the inlet of the flow domain, there are several possible ways it can affect the particle trajectories and impaction.
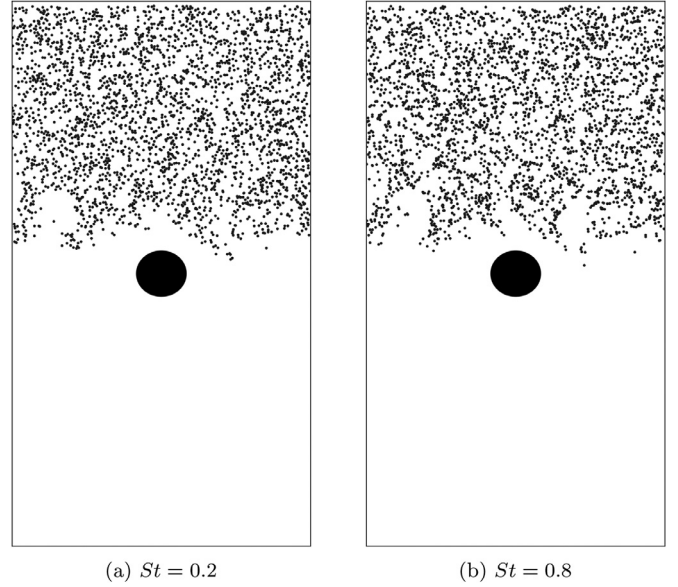

(a) $St = 0.2$ (b) $St = 0.8$

Fig. 3. Particles convected towards the cylinder in $Re = 400$ flow with free-stream turbulence with integral scale $\Lambda = 0.8D$. The thickness of the 2D-slice (in z-direction) is $12\eta_{\mathrm{Kol}}$.

3.1. The turbulence based Stokes number

The turnover time of an integral scale turbulent eddy is given as

$$\tau_e = \Lambda/u_{\mathrm{rms}}. \tag{14}$$

With this time scale a turbulence based Stokes number can be defined as $St_e = \tau_p/\tau_e$. If the eddy turnover time is much shorter than the particle Stokes time ($St_e \gg 1$) the particles are too heavy to be affected by the turbulent eddies, i.e., for large St_e the turbulence has a negligible effect on the particles. In this work, $St_e < 1.5$ for $\Lambda = 0.8D$ and $St_e < 0.5$ for $\Lambda = 2.7D$ at the inlet, so large scale effects cannot be disregarded for any of the particle sizes in use.

Alternatively, the turbulent Stokes number can be defined as $St_\eta = \tau_p/\tau_\eta$, where $\tau_\eta = \sqrt{\nu/\varepsilon}$ is the Kolmogorov time scale (with the average energy dissipation rate ε). It is known that particles with $\tau_\eta \lesssim \tau_p \lesssim \tau_e$ will experience preferential concentration (Yoshimoto and Goto, 2007), i.e. particles will cluster if $St_e \lesssim 1 \lesssim St_\eta$. The clustering has been found in low vorticity regions (Squires and Eaton, 1991). In the present study, $0.3 \lesssim St_\eta < 13.8$ ($0.1 < St_\eta \lesssim 6.6$) for $Re = 400$ ($Re = 100$). Hence, some preferential concentration should be expected, in particular for $Re = 400$ flow with particles that have particle Stokes numbers $St \gtrsim 0.7$ ($St_\eta = 0.96$ when $St = 0.7$ for this Reynolds number). Consider Fig. 3 for an illustration of preferential concentration for $St = 0.2$ and $St = 0.8$ particles. A higher degree of clustering can be seen for the larger particles (clustering takes some time to develop, and is mainly seen for particles that have been convected at least half of the upstream length). Note that corresponding plots for $Re = 100$ show no notable clustering.

3.2. Large scale turbulence

The impaction efficiency $\eta = N_{\mathrm{impact}}/N_{\mathrm{init}}$ in a laminar flow is determined by the Stokes number. Here, N_{impact} is the number of particles impacting on the cylinder surface and N_{init} is the number of particles initially positioned such that their finite radii would overlap with the cylinder at some point if convected with the mean flow in the direction of the cylinder. When $St_e \lesssim 1$, the particle trajectories will be affected by the turbulent eddies.

Consequently, the particle velocities will deviate from the mean flow velocity. When the scale of the turbulence is not small compared to the size of the cylinder, this yields a modified Stokes number, which will then also give a change in the particle impaction efficiency.

The Stokes number $St = \tau_p / \tau_f$ is by definition proportional to the mean fluid flow velocity since $\tau_f = D/2U_0$. With turbulence present in the flow, the magnitude of the flow velocity U (in general different from the mean flow velocity) is stochastic. Thus, the Stokes number is also a stochastic variable, effectively different from the *laminar St*, expressed by the uniform fluid velocity U_0. The effective Stokes number can be expressed as

$$St_{\text{eff}} = St \frac{U}{U_0}. \tag{15}$$

As St_{eff} is a linear function of U, its variance becomes

$$Var(St_{\text{eff}}) = \sigma_{St}^2 = \left(\frac{St}{U_0}\right)^2 Var(U). \tag{16}$$

Since U_0 is constant, the variance of St_{eff} is zero when $U = U_0$. The expectation value of the Stokes number is $E(St_{\text{eff}}) = St$, since U fluctuates symmetrically around the mean velocity in homogeneous isotropic turbulence.

We may re-write the effective Stokes number to $St_{\text{eff}} = St + \Delta_{St}$, where $\Delta_{St} = ((U - U_0)/U_0)St$ is the fluctuation in the Stokes number due to $U \neq U_0$. Taylor expanding the impaction efficiency yields

$$\eta(St_{\text{eff}}) = \eta(St) + \eta'(St)\Delta_{St} + \frac{\eta''(St)}{2}\Delta_{St}^2 + \mathcal{O}(\Delta_{St}^3). \tag{17}$$

The expectation value of the impaction efficiency can now be found:

$$E(\eta(St_{\text{eff}})) = \eta(St) + \eta'(St)E(\Delta_{St}) + \frac{\eta''(St)}{2}E(\Delta_{St}^2)$$
$$+ E(\eta(\mathcal{O}(\Delta_{St}^3))). \tag{18}$$

Neglecting higher order terms and using that $\sigma_{St}^2 = E(\Delta_{St}^2) - E(\Delta_{St})^2 = E(\Delta_{St}^2)$, due to the symmetry of velocity fluctuations around the mean, yields a simple expression for the expectation value of particle impaction efficiency:

$$E(\eta(St_{\text{eff}})) \approx \eta(St) + \frac{\eta''(St)}{2}\sigma_{St}^2. \tag{19}$$

When there is no turbulence $\Delta_{St} = 0$ and the expectation value of the impaction efficiency is $E(\eta(St_{\text{eff}}) = \eta(St)$. In other words, it equals the impaction efficiency in the laminar case, as anticipated.

In order to use Eq. (19) to predict particle impaction efficiencies with turbulence present, values for $\eta(St)$, $\eta''(St)$ and σ_{St}^2 are required. There are different ways to find or approximate these variables, and we suggest the following: Results for impaction efficiencies, η, are readily available in literature (see, e.g. Haugen and Kragset, 2010) and from our recent simulations. Second derivatives of these measurements can be found by curve fitting to existing results, and finding derivatives of the fitted curves. To find the effective Stokes number, the variance of U is needed. This value can be computed straightforwardly by considering the sample variance of the velocity field of the decaying turbulence. This can be done either in the flow domain, upstream of the cylinder, or in a cylinder-free domain, where the decaying turbulence is considered free from any obstructions in the flow. The latter approach is used in this study. We will return to this subject in Section 4.2.

As the impaction is also dependent on the Reynolds number, a Reynolds number dependent expectation value expression can be derived. With the same procedure for derivation as above, we get:

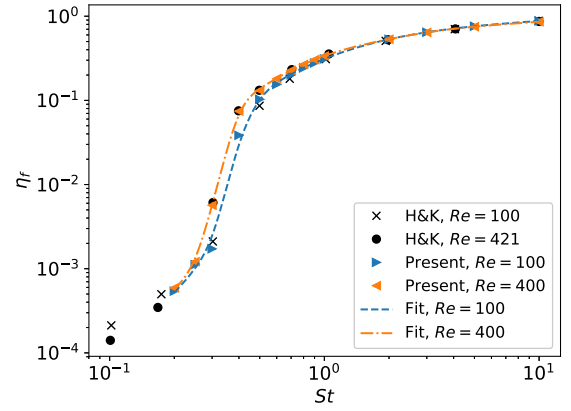$$E(\eta(Re_{\text{eff}})) \approx \eta(Re) + \frac{\eta''(Re)}{2}\sigma_{Re}^2, \tag{20}$$

Fig. 4. Front side impaction efficiency η_f for laminar free-stream flow. Present results computed in a three-dimensional domain at $Re = 100$ and 400, compared to results by Haugen and Kragset (2010) computed at $Re = 100$ and 421 in a two-dimensional domain.

where $Re_{\text{eff}} = Re(U/U_0)$ and $\sigma_{Re}^2 = Var(Re_{\text{eff}})$. To use this expression, $\eta(Re)$ and (approximations of) $\eta''(Re)$ are needed. In the present study, simulations were only performed for two different Reynolds numbers, which is insufficient to compute $\eta(Re)$ and $\eta''(Re)$. We will therefore only focus on the predictions of turbulence effects based on the effective Stokes number.

3.3. Small scale turbulence

High velocity small scale eddies may penetrate into the boundary layer around the cylinder. If this happens, and if these eddies have turnover times that are of the order of the particle response time, the particles can impact on the cylinder surface due to turbophoresis. Here, turbophoresis refer to the transport of particles from areas of high turbulent intensity to areas of low turbulent intensity (related to much larger spatial scales than preferential concentration). This could have a significant effect on the impaction efficiency. Let us call this "impaction by external turbophoresis" (see Mitra et al., 2018, and references therein for a study of non-channel-flow turbophoresis). For the low Reynolds number simulations studied here, this effect is expected to be negligible, but for high intensity high Reynolds number turbulence the turbophoretic effect may have a significant influence on the impaction efficiency for some Stokes numbers.

4. Results and discussion

As mentioned the impaction efficiency $\eta = N_{\text{impact}}/N_{\text{init}}$, where N_{init} is the total number of particles inserted over a cylinder area projected onto the flow inlet. The impaction efficiency can be considered as a sum of two parts, $\eta = \eta_f + \eta_b$, where η_f and η_b are the front- and back-side impaction efficiencies, respectively. The bulk of the particles that impact the cylinder at low and moderate Reynolds numbers do so on the front-side, and we focus only on this part of the impaction efficiency here. For back-side impaction to become significant, larger Reynolds numbers and smaller particles than used in this study must be considered. Note that the expectation value expression derived in Section 3.2 is also valid for front-side impaction, as long as all η and η'' are substituted for η_f and η_f'', respectively (the exact same steps from Eqs. (17) to (19) can be done for η_f rather than η).

To verify that the particle impaction results are sufficiently accurate, results from a flow without disturbances from free-stream turbulence are compared with results from a two-dimensional impaction study in literature. The comparison can be seen in Fig. 4,
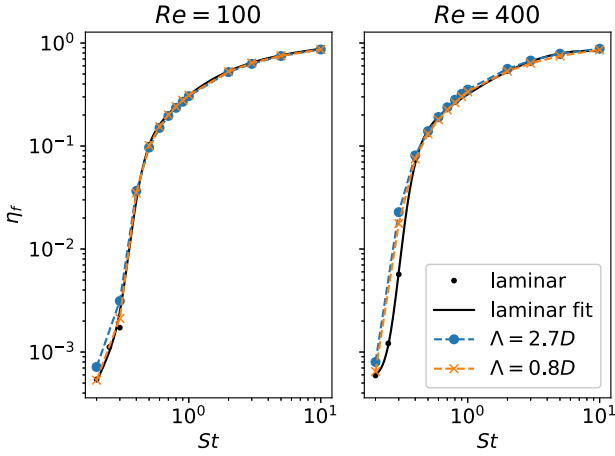
Fig. 5. Front side impaction efficiency η_f. Results for laminar and turbulent free-stream, the latter with integral scale $\Lambda = 2.7D$ or $0.8D$. Results for Reynolds numbers $Re = 100$ and 400.

where it is apparent that the earlier results are reproduced very well by the present DNS.

From Fig. 4 it is also clear that the three-dimensional effects present in the flow at $Re = 400$ do not have a noticeable impact on the front-side impaction efficiency (this would be seen as discrepancy between the present (3D) and literature (2D) results for $Re = 400$). This is not surprising, as the flow is in the upper part of the transition-in-wake regime at this Reynolds number, where three-dimensional effects occur in the wake of the cylinder, not on the front-side.

4.1. Simulations with free-stream turbulence

High-intensity turbulence was inserted at the inlet an decayed when convected downstream. The intensity of the turbulence was 22–23% at the inlet in all simulations with free-stream turbulence, and the decay was strongly dependent on integral scale and Reynolds number (see Section 2.2 for details).

Consider Fig. 5, depicting the impaction efficiencies with and without a turbulent free-stream. A few changes are apparent in the results: For certain Stokes numbers an increase in η_f can be seen, for both Reynolds numbers. The increase is largest for the largest integral scale turbulence. Further, the effect of the turbulence appears to be larger for $Re = 400$ than for $Re = 100$. These observation are not surprising, as larger effects are expected from the turbulence with higher turbulence intensity. Another, perhaps less expected consequence of the turbulence, is that the increase in impaction is largest at $St \leq 0.3$. This is in the Stokes number region where the dominant impaction mechanism changes from boundary stopping to boundary interception (as the Stokes number is decreased).

To gain further insight into the effect of the turbulence on the front-side impaction, the impaction results from particles subjected to a turbulent free-stream are normalized with corresponding results from laminar free-stream flow. The resulting amplification factor:

$$R_f = \frac{\eta_{f,\text{turb}}}{\eta_{f,\text{lam}}}, \tag{21}$$

is a direct measure of increase or decrease of impactions due to the free-stream turbulence. The amplification factor is plotted together with predicted values in Fig. 6. The predicted values will be considered in Section 4.2.

Fig. 6(a) depicts R_f as a function of Stokes number for $Re = 100$ for the two different turbulence cases considered. It is evident that
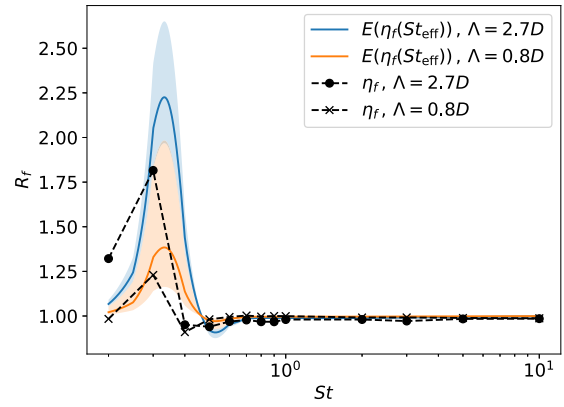
(a) $Re = 100$
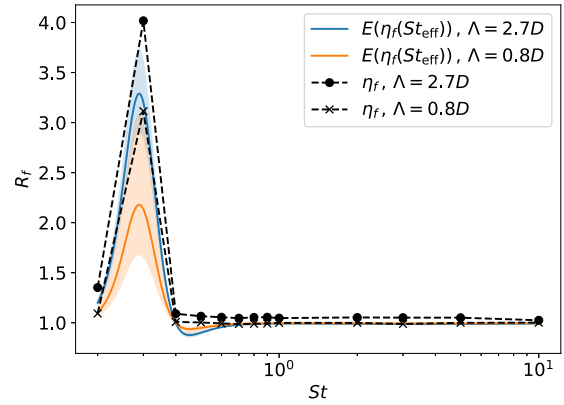
(b) $Re = 400$

Fig. 6. Predicted and observed results for amplification factor of impaction efficiencies resulting from turbulence of different integral scales interacting with particles in the flow.

the turbulence significantly increased impaction of particles in the lower range of the Stokes number domain. This is in accordance with the findings of Weber et al. (2013b), where only impaction below a critical Stokes number, St_{crit}, was affected by turbulence. For $Re = 106$, Weber et al. (2013b) computed $St_{\text{crit}} = 0.324$, which is in agreement with the $Re = 100$ simulation results, showing only a small effect of the turbulence for $St \geq 0.4$. For particles with $St \geq 0.4$ we observe a small decrease in the impaction for particles in the free-stream turbulence, with R_f approaching one as the Stokes number is increased.

Contrary to the results of Weber et al. (2013b), a distinct peak of amplification occurs at $St = 0.3$. For the larger integral scale turbulence the amplification is approximately 1.8, an increase from 0.17% impaction to 0.31% impaction. This peak can be attributed to the change in impaction mechanism, from boundary stopping to boundary interception, near this Stokes number. When particles are affected by the turbulence, they experience a change in their effective Stokes number. A small increase (decrease) in velocity will give a slightly higher (lower) Stokes number. If we take St_{peak} to be the St where the impaction mechanism changes (see Section 4.2) and consider the laminar impaction curves in Fig. 4, a particle with Stokes number $St_{\text{peak}} + \Delta_{St}$ will have a smaller chance to impact if $\Delta_{St} < 0$ (boundary interception dominating), but a much higher chance to impact if $\Delta_{St} > 0$ (boundary stopping dominating). With the mean of Δ_{St} being zero, this will result in an average increase in impaction efficiency near St_{peak}. Note that without including the boundary interception mechanism in the simulations (as in Weber et al., 2013b) the amplification $R_f \to \infty$ as

$St \rightarrow St_{\mathrm{crit}}$, and the distinct amplification peak will not be observable.

The results for $Re = 400$ (see Fig. 6(b)), are similar to those for the lower Reynolds number. Again, the amplification is greatest for particles with Stokes numbers ≤ 0.3, and there is a distinct peak in R_f at $St = 0.3$. Yet, a few differences between the results at $Re = 100$ and $Re = 400$ can be noted: the turbulence gave rise to a larger amplification effect in the latter case, and the difference between the effect from the two turbulence realizations is smaller. Neither of these findings are very surprising, if one considers that the intensity of the turbulence decayed slower in the flow domain when the Reynolds number was increased. In addition to these aspects, some amplification of the impact of larger particles is observed at $Re = 400$. This effect ($R_f = 1.02$–1.06 for $St \geq 0.5$, decreasing with increasing St) is only seen for the highest intensity case ($\Lambda = 2.7D$). In a study by Homann et al. (2016), the amplification of particle impaction on a sphere in a turbulent flow converged to unity as a power law of St (decreasing with increased St). This trend was most clear for very strong turbulent fluctuations ($T_i = 0.60$ and $T_i = 1.18$). A similar relationship can be investigated for impaction on a cylinder, but higher intensity turbulence than used in the present study is required before conclusions can be drawn. Note that impaction by boundary interception was not included in the study by Homann et al. (2016), and including such a mechanism may affect a power law trend.

The results at $Re = 100$ showed agreement with the CFD-study by Weber et al. (2013b) in terms of a cut-off Stokes number above which the turbulence played a minor role in terms of amplifying particle impaction. Weber et al. (2013b) did not report a critical Stokes number for $Re = 400$, but St_{crit} can be approximated to 0.25 for $Re = 400$, by interpolating from their reported critical Stokes numbers. Using this value as a cut-off Stokes number is, however, not consistent with our observations of effects of the free-stream turbulence for $Re = 400$. On the contrary, the peak in turbulence effect on impaction is found at the same Stokes number for $Re = 400$ as for $Re = 100$, which is above the approximated St_{crit} for $Re = 400$. The critical Stokes number as defined by Weber et al. (2013b) was intended as a limit for when zero-sized particles impact ($St > St_{\mathrm{crit}}$) or do not impact ($St < St_{\mathrm{crit}}$) the cylinder in a laminar free-stream flow. From our simulations it appears that this critical Stokes number is related to a peak amplification, when boundary interception (particles with finite radii) is included. The $St = 0.3$ particles in the $Re = 400$ flow are expected to be near this peak Stokes number. Hence, a significant amplification at $St = 0.3$ is not surprising, and an even larger amplification is expected if particles with $St = St_{\mathrm{peak}}$ were considered. Investigating this would require, first, a determination of St_{peak}.

4.2. Predictions of free-stream turbulence effects on particle impaction

In all simulations, the integral scale of the free-stream turbulence was of the same order of magnitude as the cylinder diameter. The free-stream turbulence is such that $St_e = \tau_p / \tau_e \lesssim 1$, hence, the particles should be expected to be convected by the larger turbulent eddies if the flow domain was free of any obstacles.

To be able to predict effects of the turbulence on the particle impaction, data from the turbulence-free simulations was used to compute the unknowns $\eta(St)$ and $\eta''(St)$ in Eq. (19). Flow data from simulations with a turbulent free-stream decaying in a cylinder-free domain was used to approximate σ_{St}. In the following we explain how this was done in practice.

First, the cfit-tool with smoothing splines (for $Re = 100$ results) and rational fractions (for $Re = 400$ results) in MATLAB (software version MATLAB, 2016) was used to fit curves to the impaction data computed for flow with a laminar free-stream. This yielded expressions for $\eta(St)$ in the entire Stokes number range covered by the sample of particle sizes. Different curve fitting was used for the two data sets, as this yielded the best possible fit for each set. This fitting was done in logarithmic space, hence, exponentials of the fitted results are the impaction efficiencies (displayed in Fig. 4). From a fitted function $f(\log(St)) = \log(\eta(St))$, second derivatives were found analytically by:

$$\eta''(St) = \frac{\mathrm{d}^2}{\mathrm{d}(St)^2} \exp[f(\log(St))]$$
$$= \frac{e^f}{St^2}\left[\frac{\mathrm{d}^2 f}{\mathrm{d}(\log(St))^2} + \left(\frac{\mathrm{d}f}{\mathrm{d}(\log(St))}\right)^2 - \frac{\mathrm{d}f}{\mathrm{d}(\log(St))} \right].$$
(22)

Finally, the variance of the upstream velocity field, necessary to compute σ_{St} by Eq. (16), was needed. Since the Reynolds numbers were moderate, the turbulence decayed quite rapidly. Hence, the variance of the velocity depended strongly on where in the flow domain the velocity was measured. Since we are interested in the stochastic property of the velocity due to the turbulence only, the variance was computed in a flow domain without a cylinder present. To obtain relevant values for the computations, the variance was averaged at each grid point in time and moving averages were computed in the streamwise direction. The moving averages were computed over a $0.5D$ thick slab in the streamwise direction, starting a distance $0.5D$ downstream of the inlet, and continuing to where the center of the cylinder would be positioned if the cylinder was present. Mean, maximum and minimum values of the moving averages were found and used as prediction and prediction bounds of $Var(U)$.

The amplification factors predicted by inserting the computed $\eta(St)$, $\eta''(St)$ and σ_{St} in Eq. (19) can be seen as the colored areas in Fig. 6. Quite large error bounds are used, due to the way the variance was computed (as noted in the previous paragraph). The predictions fit well with the DNS impaction results. In particular, the strong amplification of the impaction efficiencies close to $St = 0.3$ is predicted by the statistical analysis. From Eq. (19) the observed amplification of particle impaction is not surprising for the Stokes numbers where the impaction curves are concave up. Haugen and Kragset (2010) showed that the impaction efficiency is close to linear in the boundary interception mode. Hence, the second derivative of $\eta(St)$ with respect to Stokes number will be approximately zero in this region. Based on the expression for predicted impaction we would therefore not expect a significant effect of turbulence on inertial impaction in the boundary interception regime (but a strong effect in the region where impaction mechanism changes from boundary stopping to boundary interception).

The predictions (Fig. 6) show that the amplification is greatest for particles with $St = 0.33$ for $Re = 100$ and $St = 0.29$ for $Re = 400$. We identify these Stokes numbers as measures for St_{peak} for the particle sizes used in the present cases. Note that St_{peak} is close to, but somewhat larger than, the critical Stokes numbers for its respective Reynolds number. This is in accordance with the suggested explanation that the boundary interception becomes the dominant impaction mechanism at St_{peak}. With zero-sized particles, $\eta(St) \rightarrow 0$ as $St \rightarrow St_{\mathrm{crit}}$. With finite-sized particles, $\eta(St)$ decreases towards zero in the same way, when the Stokes number is reduced in the boundary stopping impaction regime. The trend is interrupted for $St = St_{\mathrm{peak}} > St_{\mathrm{crit}}$, for which a significant amount of particles impact by boundary interception. Boundary interception is dependent on the particle radii, and, hence, so is St_{peak}. Consider, e.g. particles with half the density ρ_p of the particles in the present study, with all other parameters (except size) unchanged. The particles will have a 40% larger radius than particles in the present study (see Eq. (11)). Consequently, impaction by boundary interception is more likely to occur, and a larger St_{peak} is expected.

For the larger particles $(St \gtrsim 0.5)$ the predictions by Eq. (19) show a convergence to unity from below (impaction curve $\eta(St)$ is concave down, yielding $\eta''(St) < 0$). The results from turbulence simulations yielded $\eta(St > 0.5) \simeq 1$, approached from below, for $\Lambda = 0.8D$ turbulence for both Reynolds numbers. A similar trend is found for $\Lambda = 2.7D$ turbulence for $Re = 100$, yet here approximately 3–1% decrease $(R_f \approx 0.97$–$0.99)$ was measured for $St = 0.6$–10 (R_f closer to 1 for higher Stokes numbers). Only with the large scale turbulence for $Re = 400$ was the trend $R_f \to 1$ from below contradicted. As mentioned in Section 4.1, amplification of 2–6% for $St = 0.5$–10 (smaller amplification for higher Stokes numbers) was observed for this case. This contradicts the predictions by Eq. (19), yet is in accordance with observations by Homann et al. (2016) that found increased impaction (on a sphere) for all St when the free-stream was turbulent. Nevertheless, we have seen that the predictive expression fits well with our data for $St < 0.5$. The inability to predict amplification of impaction at higher Stokes numbers for $Re = 400$ and $\Lambda = 2.7D$ may be due to assumptions made when deriving Eq. (19) being invalid for such cases. One possibility is that the preferential concentration of these particles in low vorticity zones affected the velocity fluctuations experienced by the particles. Although the velocity fluctuations of the flow field were symmetric (yielding $E(\Delta_{St}) = 0$), preferential concentration may have lead particles to experience a non-symmetric velocity field. Consequently, the odd derivatives of $\eta(St)$ in (Eq. (18)) should not cancel in the Taylor expansion of $\eta(St_{eff})$. Note also, that the higher order terms in the Taylor expansion cannot be neglected if large particles are affected by turbulence with very high intensity, since this may yield $\sigma_{St} > 1$. Consider e.g., that turbulence with intensity decaying such that $Var(U)/U_0^2 \geq 1$ yields $\sigma_{St} \geq 1$ for $St \geq 1$. This was not the case here, but should be considered by other researchers who would like to use Eq. (19) to predict effects of turbulence on particle impaction.

5. Conclusion

The effect of free-stream turbulence on inertial particle impaction for a large range of Stokes numbers has been investigate by DNS. The following can been concluded from the study:

(a) The effect that free-stream turbulence has on the impaction rate of particles on a cylinder depends largely on the particle Stokes number. There is a peak Stokes number for which the largest amplification of particle impaction on the cylinder occurs. For the sample of Stokes numbers used in the present study, $St = 0.3$ was closest to the peak Stokes number, in both $Re = 100$ and $Re = 400$ flow. The relative increase in particle impaction decreases fast when the difference between a particle's Stokes number and the peak Stokes number increases.

(b) The peak Stokes number is related to where the impaction mechanism changes from being dominated by boundary stopping $(St > St_{peak})$ to boundary interception $(St < St_{peak})$. At which Stokes number impaction by boundary interception becomes the dominating impaction mechanism depends on the size of the particles for a given Stokes number. Hence, St_{peak} is not a fixed value depending only on St. The value will depend on the parameters that make up the Stokes number.

(c) The effect of turbulence on particle impaction is also dependent on the Reynolds number of the flow, and the intensity and integral scale of the turbulence. The Reynolds number and the integral scale of the turbulence determine how fast the intensity of the turbulence decays in the flow domain. Higher Reynolds number and larger integral scale (i.e., higher turbulence intensity) yield a larger amplification of

impaction. In the present study, the Reynolds number and integral scale effects cannot be distinguished from the turbulence intensity effects. Hence the study is inconclusive in regards to how these parameters individually will effect the amplification of impaction.

(d) Using St_{crit} as a measure of for which particles with $St < St_{crit}$ experience the largest effects of the free-stream turbulence on impaction is not appropriate when boundary interception is included as an impaction mechanism. For finite-sized particles, the peak Stokes number, where the maximum effect of the turbulence on particle impaction is found, will always be larger than St_{crit}.

(e) A quite simple expression for the expected turbulence effects on impaction was derived:

$$E(\eta(St_{eff})) \approx \eta(St) + \frac{\eta''(St)}{2}\sigma_{St}^2.$$

Comparison of predicted effects from this expression with DNS results was favorable, in particular in the lower Stokes number region.

Based on our conclusions, we suggest three topics of further research. Firstly, the largest impaction was observed at $St = 0.3$. This is slightly below the predicted peak for $Re = 100$ and slightly above for $Re = 400$. Increasing the St-resolution in this region, that is, performing additional simulations with a large number of particles distributed among Stokes numbers ranging from 0.2 to 0.4 could to a greater extent pinpoint a the Stokes number where the maximum turbulence effect on impaction occurs. This would be useful in a further validation of the model for predicting particle impaction in a turbulent flow. This would also increase the accuracy of the fitted laminar $\eta_f(St)$ curves, giving better predictions based on expectation values. Secondly, the Reynolds number should be increased both to see if the Stokes number of the peak is shifted, and to further investigate the effect of the turbulence integral scale when separated from intensity. Along with this, the inlet turbulence intensity should be varied for a fixed integral scale, such that distinct effects of T_i can be identified. Thirdly, extending this study to much smaller particle sizes would make it possible to consider if effect of turbulence diminishes for very small particles and, further, to explore turbulence effects on backside impaction. The back-side impaction phenomenon has previously been found by Haugen and Kragset (2010) to occur for small particles $(St \lesssim 0.13)$, for $Re \geq 400$. For very small particles effects of thermophoresis should be taken into account, as recent studies (Beckmann et al., 2016; García Pérez et al., 2016) have found that such mechanisms to be very important for particle transport and deposition of small particles.

References

Aarnes, J.R., Andersson, H.I., Haugen, N.E.L., 2018. Numerical investigation of free-stream turbulence effects on the transition-in-wake state of flow past a circular cylinder. J. Turbul. 19 (3), 252–273.

Beckmann, A.M., Mancini, M., Weber, R., Seebold, S., Müller, M., 2016. Measurements and CFD modeling of a pulverized coal flame with emphasis on ash deposition. Fuel 167, 168–179.

Brandenburg, A., 2001. The inverse cascade and nonlinear alpha-effect in simulations of isotropic helical hydromagnetic turbulence. Astrophys. J. 550 (2), 824.

Brandenburg, A., Dobler, W., 2002. Hydromagnetic turbulence in computer simulations. Comput. Phys. Commun. 147 (1–2), 471–475.

Cunningham, E., 1910. On the velocity of steady fall of spherical particles through fluid medium. Proc. R. Soc. Lond. A 83 (563), 357–365. doi:10.1098/rspa.1910.0024.

Davies, C., 1945. Definitive equations for the fluid resistance of spheres. Proc. Phys. Soc. 57 (4), 259.

Douglas, P.L., Ilias, S., 1988. On the deposition of aerosol particles on cylinders in turbulent cross flow. J. Aerosol. Sci. 19 (4), 451–462.

García Pérez, M., Vakkilainen, E., Hyppänen, T., 2016. Unsteady CFD analysis of kraft recovery boiler fly-ash trajectories, sticking efficiencies and deposition rates with a mechanistic particle rebound-stick model. Fuel 181, 408–420.

Haugen, N.E.L., Brandenburg, A., 2006. Hydrodynamic and hydromagnetic energy spectra from large eddy simulations. Phys. Fluids 18 (7), 075106.

Haugen, N.E.L., Kragset, S., 2010. Particle impaction on a cylinder in a crossflow as function of Stokes and Reynolds numbers. J. Fluid Mech. 661, 239–261.

Haugen, N.E.L., Kragset, S., Bugge, M., Warnecke, R., Weghaus, M., 2013. MSWI super heater tube bundle: particle impaction efficiency and size distribution. Fuel Process. Technol. 106, 416–422.

Homann, H., Guillot, T., Bec, J., Ormel, C., Ida, S., Tanga, P., 2016. Effect of turbulence on collisions of dust particles with planetesimals in protoplanetary disks. Astron. Astrophys. 589, A129.

Huang, L., Norman, J., Pourkashanian, M., Williams, A., 1996. Prediction of ash deposition on superheater tubes from pulverized coal combustion. Fuel 75 (3), 271–279.

Ingham, D.B., Hildyard, L.T., Hildyard, M.L., 1990. On the critical stokes' number for particle transport in potential and viscous flows near bluff bodies. J. Aerosol. Sci. 21 (7), 935–946.

Israel, R., Rosner, D.E., 1982. Use of a generalized Stokes number to determine the aerodynamic capture efficiency of non-stokesian particles from a compressible gas flow. Aerosol Sci. Technol. 2 (1), 45–51.

Kasper, G., Schollmeier, S., Meyer, J., Hoferer, J., 2009. The collection efficiency of a particle-loaded single filter fiber. J. Aerosol. Sci. 40 (12), 993–1009.

Li, X., Zhou, H., Cen, K., 2008. Influences of various vortex structures on the dispersion and deposition of small ash particles. Fuel 87 (7), 1379–1382.

Lodato, G., Domingo, P., Vervisch, L., 2008. Three-dimensional boundary conditions for direct and large-eddy simulation of compressible viscous flows. J. Comput. Phys. 227 (10), 5105–5143. doi:10.1016/j.jcp.2008.01.038.

MATLAB, 2016. Matlab and Statistics Toolbox Release 2016a. MathWorks, Inc., Massachusetts, United States.

Mitra, D., Haugen, N.E.L., Rogachevskii, I., 2018. Turbophoresis in forced inhomogeneous turbulence. Eur. Phys. J. Plus 133 (2), 35.

Phillips, C., Kaye, S., 1999. The influence of the viscous boundary layer on the critical Stokes number for particle impaction near a stagnation point. J. Aerosol. Sci. 30 (6), 709–718.

Poinsot, T.J., Lele, S., 1992. Boundary conditions for direct simulations of compressible viscous flows. J. Comput. Phys. 101 (1), 104–129.

Schweers, E., Umhauer, H., Löffler, F., 1994. Experimental investigation of particle collection on single fibres of different configurations. Particle Particle Syst. Charact. 11 (4), 275–283.

Squires, K.D., Eaton, J.K., 1991. Preferential concentration of particles by turbulence. Phys. Fluids A 3 (5), 1169–1178.

The Pencil Code, 2018. ⟨pencil-code.nordita.org [Internet]⟩. Stockholm (SE): NORDITA; [updated January 2018]. Available from: https://github.com/pencil-code.

Weber, R., Mancini, M., Schaffel-Mancini, N., Kupka, T., 2013a. On predicting the ash behaviour using computational fluid dynamics. Fuel Process. Technol. 105, 113–128.

Weber, R., Schaffel-Mancini, N., Mancini, M., Kupka, T., 2013b. Fly ash deposition modelling: requirements for accurate predictions of particle impaction on tubes using RANS-based computational fluid dynamics. Fuel 108, 586–596.

Williamson, C.H.K., 1996. Vortex dynamics in the cylinder wake. Annu. Rev. Fluid Mech. 28, 477–539.

Williamson, J., 1980. Low-storage Runge–Kutta schemes. J. Comput. Phys. 35 (1), 48–56.

Yilmaz, S., Cliffe, K., et al., 2000. Particle deposition simulation using the CFD code FLUENT. J. Inst. Energy 73 (494), 65–68.

Yoo, C.S., Wang, Y., Trouvé, A., Im, H.G., 2005. Characteristic boundary conditions for direct simulations of turbulent counterflow flames. Combust. Theor. Model. 9 (4), 617–646.

Yoshimoto, H., Goto, S., 2007. Self-similar clustering of inertial particles in homogeneous turbulence. J. Fluid. Mech. 577, 275–286.